Electromagnetic retrieval of missing fibers in periodic fibered laminates via sparsity concepts

Zi-Cheng Liu*, Chang-You Li†, Dominique Lesselier*, and Yu Zhong‡
*Laboratoire des Signaux et Systèmes
CNRS-CentraleSupélec-U. Paris Sud, Université Paris Saclay, France
zicheng.liu@l2s.centralesupelec.fr, dominique.lesselier@l2s.centralesupelec.fr
†BioMedical-Electromagnetics Group, Engineering Product Department
Singapore University of Technology and Design, Singapore
changyou_li@sutd.edu.sg
‡A*STAR, Institute of High Performance Computing, Singapore
zhongyu@ihpc.a-star.edu.sg

***Abstract*—Electromagnetic modeling and imaging of fibered laminates with some fibers missing is investigated, this extending to similarly organized photonic crystals. Parallel circular cylinders are periodically set in a homogeneous layer (matrix) sandwiched between two homogeneous half-spaces. Absent fibers destroy the periodicity. An auxiliary periodic structure (supercell) provides a subsidiary model considered using method tailored to standard periodic structures involving the Floquet theorem to decompose the fields. Imaging approaches from the Lippman-Schwinger integral field formulation as one-shot MUltiple SIgnal Classification (MUSIC) with pointwise scatterers assumptions and an iterative, sparsity-constrained solution are developed. Numerical simulations illustrate the direct model and imaging.**

I. Introduction

Fiber-reinforced composite laminates are widely used for their advantages in terms of stiffness and strength in man-made parts in aeronautics, automotive industry and for green energy applications. Ensuring reliable usage is necessary, and challenging issues of non-destructive testing (NdT) appear.

Electromagnetic means of testing are one option among many others, here from MHz to THz operation frequencies depending upon the characteristics of the laminates. Also due to similarities of organization, methods developed for such composites extent to photonic crystals, e.g., [1]. To succeed, both accurate forward models and stable inversion algorithms are needed, as shown for fibers in air [2], [3], [4].

The laminates which one is concerned with are made of finitely-thick planar layers set between two homogeneous half-spaces. Within each layer (matrix), longitudinally-orientated circular cylindrical fibers of same cross-section are periodically embedded to infinity along the transverse direction, fiber orientations being expected to differ from one layer to another.

For most methods for analyzing periodic structures as in aforementioned contributions and references including in particular [5], the Floquet theorem is applied from the field pseudo-periodicity so that the field analysis can be concentrated onto the primary unit. However, since the periodicity is destroyed from absent fibers, this prior knowledge becomes irrelevant. This can be tackled by introducing an auxiliary new periodic structure with each unit (supercell) defined as multiple fibers and defects in the central area. Enlarging the number of contained fibers, the field within, above and below the central region of the supercell should converge to the true field.

As is well-known, compressive sensing uses the sparsity of signals to achieve high-resolution imaging [6]. Since, in the cases here, only a few fibers are missing within the explored region, sparsity lies with the fiber distribution, and that can be employed to locate them.

Based on an imaging model derived from the Lippman-Schwinger field integral formulation [2], an optimization problem about the fiber distribution can be proposed by regularizing the sparsity with l_1-norm and constraining the data residual by l_2-norm. In addition, a preconditioning procedure is applied on the sensing matrix to deal with ill-posedness.

In parallel, standard one-shot MUSIC imaging, for which sparsity is inherent due to the assumption of well-separated pointwise scatterers, is developed and compared.

II. Analysis of electromagnetic behavior

The structure is sketched in Fig. 1. An infinite set of circular cylindrical fibers orientated into the y direction is embedded in a planar layer with upper and lower interfaces $z = a$ and $z = b$. They are periodically arranged with period d and of radius c. The space is divided into R_{0+} and R_{0-} for regions above and below the layer, R for the matrix containing the fibers, and R_l for fiber l. All materials are linear isotropic.

Relative dielectric permittivity and magnetic permeability are ϵ_j, μ_j, $j = 0+, 0-, \cdot, l, \cdot$ standing for null. Fibers are with $\epsilon_l = \epsilon_f, \mu_l = \mu_f$ except absent ones with then $\epsilon_l = \epsilon, \mu_l = \mu$, subscript f denoting fiber material.

Two types of sources are considered thereafter (harmonic time-dependence $-i\omega t$ implied): a E-polarized (TM) plane wave obliquely illuminating the laminate with angle θ^{inc} and field $\mathbf{E}_y^{inc}(\mathbf{r}) = \hat{y}E_y^{inc}e^{i[\alpha_0 x - \beta_0(z-a)]}$, $\mathbf{r} = (x, z)$ observation point, $\alpha_0 = k_{0+}\sin\theta^{inc}$, $\beta_0 = k_{0+}\cos\theta^{inc}$, k_j wavenumber, and E_y^{inc} amplitude set as unity; a line source set inside the fiber with position $\mathbf{r}_s$ and expression $1/4iH_0^{(1)}(k_l|\mathbf{r} - \mathbf{r}_s|)$ ($H_0^{(1)}$ first-kind Hankel function of order 0).

978-0-9928-6265-7/16/$31.00 ©2016 IEEE

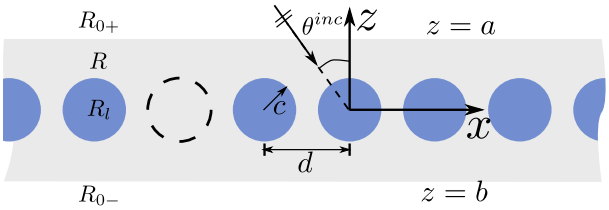

Fig. 1. Cross-section of single-layer laminate with a missing fiber.

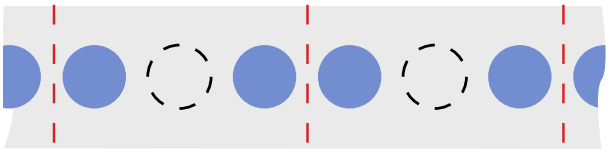

Fig. 2. Sketch of the auxiliary periodic structure based on supercell, $L=3$.

Without fibers missing, the structure is periodic and the field analysis can be concentrated onto the primary unit by applying the Floquet theorem. Yet, as said, the periodicity is destroyed by absent fibers.

An auxiliary new periodic structure can be introduced as follows: truncate the laminate to get a cell (called supercell) including multiple fibers and missing fibers located within the central area, as the region bounded by dashed lines in Fig. 2; repeat this cell along the line connecting the centers of fiber cross-sections. A new periodic structure follows and its analysis can be led accordingly.

Let the number of contained fibers (including the missing ones) in the supercell be L; according to the Floquet theorem, $E_y(x+D,z) = E_y(x,z)\,e^{i\alpha_0 D}$ [7], $D=Ld$, then the field above and below the layer can be plane-wave expanded as

$$E_y^{0+}(\vec{r}) = \sum_{p\in\mathbb{Z}} \left[\delta_p e^{-i\beta_p^{0+}(z-a)} + r_p e^{i\beta_p^{0+}(z-a)}\right] e^{i\alpha_p x}, \quad (1)$$

$$E_y^{0-}(\vec{r}) = \sum_{p\in\mathbb{Z}} t_p e^{-i\beta_p^{0-}(z-b)} e^{i\alpha_p x}, \quad (2)$$

where r_p and t_p represent the reflection and transmission coefficients for the p-th plane-wave component, δ_p is a Kronecker delta, $\alpha_p = \alpha_0 + 2\pi p/D$, $\beta_p^j = \sqrt{(k_j)^2 - \alpha_p^2}$.

The field in the matrix is a combination of field scattered by the layer interfaces and fibers. Representing the field inside and in the vicinity of the l-th fiber via multipole expansions,

$$E_y(\vec{r}) = \sum_{m\in\mathbb{Z}} \left[A_m^l J_m(kr_l) + B_m^l H_m^{(1)}(kr_l)\right] e^{im\theta_l}, \quad (3)$$

$$E_y(\vec{r}) = \sum_{m\in\mathbb{Z}} \left[C_m^l J_m(k_l r_l) + Q_m^l H_m^{(1)}(k_l r_l)\right] e^{im\theta_l}, \quad (4)$$

where $Q_m^l = \chi_l / i4 J_m(k_l r_l^s) e^{-im\theta_l^s}$ are for the line source inside the fiber, (r_l, θ_l) and (r_l^s, θ_l^s) are local coordinates of $\mathbf{r}$ and $\mathbf{r}_s$ with respect to the system originated at the center of the l-th fiber, and J_m and $H_m^{(1)}$ are the first-kind Bessel and Hankel function of order m. χ_l valued to 1 implying the presence of interior source, and 0 otherwise.

Making use of the periodic Green's function

$$G(\vec{r}) = \frac{1}{i2D} \sum_{p\in\mathbb{Z}} \frac{1}{\beta_p} e^{i[\alpha_p x + \beta_p |z|]} \quad (5)$$

and applying the Green's theorem along the boundary of the primary supercell, the field in R can be expressed as

$$\begin{aligned} E_y(\vec{r}) = &\sum_{p\in\mathbb{Z}} \left[f_p^- e^{-i\beta_p z} + f_p^+ e^{i\beta_p z}\right] e^{i\alpha_p x} \\ &+ \sum_{p\in\mathbb{Z}} \sum_{m\in\mathbb{Z}} K_{m,p}^{\pm} F_m^p e^{i(\alpha_p x \pm \beta_p z)}, \end{aligned} \quad (6)$$

$K_{m,p}^{\pm} = 2(-i)^m e^{\pm im\theta_p}/(D\beta_p)$, $F_m^p = \sum_{l=1}^L B_m^l e^{-i\alpha_p l d}$ is the discrete Fourier transform of B_m^l. With (1), (2) and (6), matching the field at the layer boundaries yields

$$\begin{aligned} r_p = &\sum_{m\in\mathbb{Z}} \sum_{l=1}^L \Pi_m^l B_m^l + \delta_p \left[w_p(w_p^{0+} - w_p^{0-})\cos(\beta_p\zeta)\right. \\ &\left. -i(w_p^{0+} w_p^{0-} - w_p^2)\sin(\beta_p\zeta)\right]/\Lambda_p \end{aligned} \quad (7)$$

$$t_p = \sum_{m\in\mathbb{Z}} \sum_{l=1}^L \Xi_m^l B_m^l + 2\delta_p w_p^{0+} w_p / \Lambda_p \quad (8)$$

and the solution of f_p^-, f_p^+ as a function of F_m^p (or B_m^p).

As the incoming wave upon the l-th fiber is composed of fields scattered by all other fibers and layer boundaries, the Rayleigh identities can be obtained in the same way with (6),

$$A_m^l = \sum_{p\in\mathbb{Z}} e^{i\alpha_p l d}\left(J_{m,p}^+ f_p^+ + J_{m,p}^- f_p^-\right) + \sum_{j=1}^L \sum_{n\in\mathbb{Z}} S_{m,n}^{lj} B_n^j \quad (9)$$

where $J_{m,p}^{\pm} = (i)^m exp(\mp im\theta_p)$, and $S_{m,n}^{lj}$ is the relative lattice sum [8] weighting the contribution from the j-th fiber.

Substituting the expression $f_p^+(B_m^l)$ and $f_p^-(B_m^l)$ into (9), a linear relationship between A_m^l and B_m^l is established,

$$A_m^l = \sum_{j=1}^L \sum_{n\in\mathbb{Z}} \left(S_{m,n}^{l,j} + \Psi_{m,n}^{l,j}\right) B_n^j + K_m^l \quad (10)$$

Together with another one from the fiber boundary conditions,

$$B_m^l = R_m^l A_m^l + T_m^l Q_m^l. \quad (11)$$

the solution of B_m^l can be written as

$$\mathbf{B} = (\mathbf{I} - \mathbf{R}\boldsymbol{\Theta})^{-1}(\mathbf{R}\mathbf{K} + \mathbf{T}\mathbf{Q}) \quad (12)$$

where column vectors $\mathbf{A} = [A_m^l]$, $\mathbf{B} = [B_m^l]$, $\mathbf{K} = [K_m^l]$, $\mathbf{Q} = [Q_m^l]$ and matrix $\boldsymbol{\Theta} = [S_{m,n}^{l,j} + \Psi_{m,n}^{l,j}]$, $\mathbf{R} = [R_m^l]$, $\mathbf{T} = [T_m^l]$, and r_p and t_p can be calculated by (7) and (8).

III. Construction of the Imaging Model

A. Imaging model for localizing the missing fibers

The disturbance of the background field due to missing fibers can be evaluated thanks to the Lippman-Schwinger integral formulation

$$\widetilde{E}_y(\mathbf{r}) - E_y(\mathbf{r}) = \sum_{l=1}^L \int_{D_l} G(\mathbf{r},\mathbf{r}')\left(k_l^2 - k_f^2\right)\widetilde{E}_y(\mathbf{r}')\,d\mathbf{r}' \quad (13)$$

where E_y denotes the total field by the well-organized structure and parameters with '$\sim$' above are associated with the disorganized one, D_l is the cross-sectional area of the l-th fiber, and $G(\mathbf{r},\mathbf{r}')$ is the field response (Green's function) when the line source is at $\mathbf{r}'$ and the laminate is well-organized. Since $k_l = k_f$ for existing fibers, which cancells the involved integral, only absent ones contribute to the disturbance.

Let the observation point $\mathbf{r}$ be above the layer. Combining (1), (7) and (12), $G(\mathbf{r},\mathbf{r}')$ follows with $\delta_p = 0$ and $\chi_l = 1$,

$$G(\mathbf{r},\mathbf{r}') = \frac{1}{4i}\sum_{m\in\mathbb{Z}} \mathbf{\Phi}_m^l(\mathbf{r}) J_m(k_f r_l') e^{-im\theta_l'} \tag{14}$$

with $\mathbf{\Phi} = \mathbf{\Gamma\Pi}\left(\mathbf{I}-\mathbf{R\Theta}\right)^{-1}\mathbf{T}$, $\mathbf{\Gamma} = \left[e^{i\left(\alpha_p x+\beta_p^{0+}(z-a)\right)}\right]$, and $\mathbf{\Pi} = \left[\Pi_m^l\right]$.

Letting $\widetilde{E}_y = \sum_{m\in\mathbb{Z}} \widetilde{C}_m^l J_m(k_l r_l')$. and substituting this expression and $G(\mathbf{r},\mathbf{r}')$ into the integration of (13), one has

$$\widetilde{E}_y(\mathbf{r}) - E_y(\mathbf{r}) = \sum_{m\in\mathbb{Z}} \mathbf{\Phi}_m^l(\mathbf{r}) q_m^l, \tag{15}$$

where $q_m^l = [k_l J_{m+1}(k_l c)J_m(k_f c) - k_f J_m(k_l c)J_{m+1}(k_f c)] \cdot \pi c \widetilde{C}_m^l / (2i)$, which is nonzero when the l-th fiber is defective and 0 otherwise. Denoting $\mathbf{q} = [q_m^l]$, (15) can be written as

$$\widetilde{E}_y(\mathbf{r}) - E_y(\mathbf{r}) = \mathbf{\Phi q}. \tag{16}$$

Assuming N_s sources and N_r receivers, for the ν-th source, the sampling data of $\widetilde{E}_y(\mathbf{r}) - E_y(\mathbf{r})$ can compose a column vector $\mathbf{y}_\nu$ with dimension N_r, $\nu = 1, 2, \ldots, N_s$. Taking y_ν as columns, the data matrix $\mathbf{Y}$ can be constructed as $\mathbf{Y} = [\mathbf{y}_1, \mathbf{y}_2, \ldots, \mathbf{y}_{N_s}]$. Since $\mathbf{\Phi}$ is invariant with the sources, an initial imaging model can be derived as

$$\mathbf{Y} = \mathbf{\Phi F}, \tag{17}$$

where $\mathbf{F} = [\mathbf{q}_1, \mathbf{q}_2, \ldots, \mathbf{q}_{N_s}]$.

B. Zero-mode approximation

Since the number of involved modes cannot be infinite in multipole expansions, $\sum_{m=-\infty}^{\infty}$ is truncated as $\sum_{m=-M}^{M}$ with $M = \text{int}\left((k_f c)^{1/3} + k_f c\right)$ [2], in which int is the operator yielding the integer part. With a low-frequency source, $(k_f c)^{1/3} + k_f c$ can be smaller than 1, then M tends to 0.

An approximated imaging model follows by letting $M = 0$:

$$\mathbf{Y} = \mathbf{\Phi}^0\mathbf{F}^0 + \mathbf{N}^0, \tag{18}$$

where superscript 0 identifies matrices only including the zero-th mode, and $\mathbf{N}^0$ is the resulting approximation error.

Benefiting from this approximation, the dimensions of the matrices involved are considerably reduced, which lightens the burden of the following imaging procedures.

Taking into account additive noise $\mathbf{N}_a$ in the data, and setting $\mathbf{Z} = \mathbf{\Phi}^0$, $\mathbf{S} = \mathbf{F}^0$ and $\mathbf{N} = \mathbf{N}^0 + \mathbf{N}_a$ for convenience, one gets the imaging model in the noisy case as

$$\mathbf{Y} = \mathbf{ZS} + \mathbf{N}. \tag{19}$$

The goal is to find the solution of $\mathbf{S}$ since the indices of missing fibers are given by the positions of its non-zero rows.

IV. Imaging methods

Standard MUSIC and the sparsity-based method are adopted to solve for $\mathbf{S}$ in (19). The literature about the former is abundant, [9], so only the latter is discussed in some detail.

A. MUSIC

Singular value decomposition (SVD) of the matrix $\mathbf{Y}$ reads as$\mathbf{Y} = \mathbf{ULV}^*$, where $*$ denotes the conjugate transpose, and $\mathbf{L}$ is a diagonal matrix composed of the singular values. According to the distribution of singular values [10], $\mathbf{U}$ is divided into signal $\mathbf{U}_s$ and noise $\mathbf{U}_n$ spaces. The estimation function of interest is

$$\hat{s}^l = \frac{\mathbf{Z}_l\mathbf{Z}_l^*}{\mathbf{Z}_l^*\mathbf{U}_n\mathbf{U}_n^*\mathbf{Z}_l}, \tag{20}$$

where $\mathbf{Z}_l$ indicates the l-th column of $\mathbf{Z}$. Since the denominator goes to zero when the l-th fiber is missing, they are shown as peaks in the curve of vector $\hat{\mathbf{s}} = [\hat{s}^l]$.

B. Sparsity-based method

In general applications, only few fibers are faulty (missing), which leads to the sparsity of $\mathbf{S}$, meaning a few nonzero elements in $\mathbf{S}$. To take advantage of this strong prior knowledge, a regularization can be enforced on $\mathbf{S}$ by minimizing its l_0-norm, which counts the number of non-zero elements, and the solution can be obtained by the following optimization:

$$\min J\left(\overline{\mathbf{S}}\right) = ||\overline{\mathbf{Y}} - \overline{\overline{\mathbf{Z}}}\overline{\mathbf{S}}||_2^2 + \tau||\overline{\mathbf{S}}||_0, \tag{21}$$

where the overline denotes the vectorization by taking columns one under another, $\overline{\overline{\mathbf{Z}}} = \mathbf{I}\otimes\mathbf{Z}$, $\otimes$ denotes the Kronecker product, and τ is the parameter trading off sparsity and data residual constrained by the l_2-norm. As usual a large τ means that $\overline{\mathbf{S}}$ tends to exhibit sharp peaks, whereas a small one is appropriate to little data pollution.

Yet, solving (21) is qualified as a NP-hard problem [11], requiring enumeration of all possible locations of nonzero entries in $\mathbf{S}$. According to [12], optimization based on l_1-norm,

$$\min J\left(\overline{\mathbf{S}}\right) = ||\overline{\mathbf{Y}} - \overline{\overline{\mathbf{Z}}}\overline{\mathbf{S}}||_2^2 + \tau||\overline{\mathbf{S}}||_1, \tag{22}$$

can also exactly recover $\mathbf{S}$ when sufficient data are collected, the solution being a saddle point due to convexity. To avoid the singularity of the l_1-norm at the origin, a smooth approximation to the l_1-norm is used:

$$||\overline{\mathbf{S}}||_1 \approx \sum_{j=1}^{L\cdot N_s}\left(\left|\left(\overline{\mathbf{S}}\right)_j\right|^2 + \varepsilon\right)^{1/2}. \tag{23}$$

where ε is a positive constant in case of zeros in $\overline{\mathbf{S}}$.

Taking the gradient of the penalty function in (22) and equating to zero yield the following estimator,

$$\left(2\overline{\overline{\mathbf{Z}}}^*\overline{\overline{\mathbf{Z}}} + \tau\Delta\left(\overline{\mathbf{S}}^{(n)}\right)\right)\overline{\mathbf{S}}^{(n+1)} = 2\overline{\overline{\mathbf{Z}}}^*\overline{\mathbf{Y}}, \tag{24}$$

where $\Delta(\overline{\mathbf{S}}^{(n)}) = \text{diag}\{\left(|(\overline{\mathbf{S}}^{(n)})_j|^2 + \varepsilon\right)^{-1/2}\}$. Equation (24) defines the iterate $\overline{\mathbf{S}}^{(n+1)}$ as solution of a linear system of equations gotten, e.g., by a Conjugate Gradient algorithm.

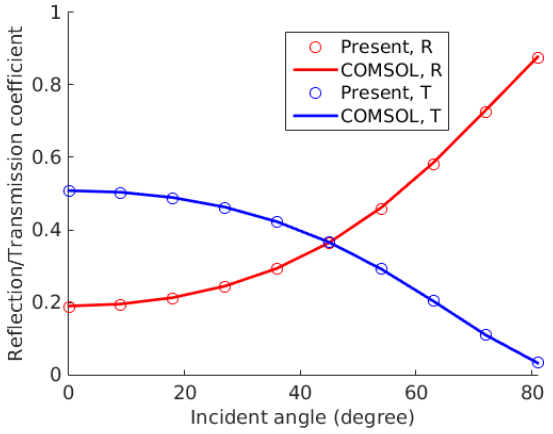

Fig. 3. Validation of modeling with different incident angles.

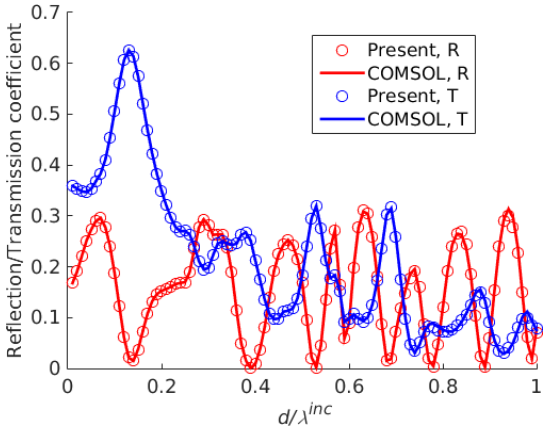

Fig. 4. Validation of modeling with different frequencies.

Note that ε should be small enough not to affect the behavior of the solution; however, too small ε may cause ill-conditioned $\Delta(\bar{\mathbf{S}}^{(n)})$. $\varepsilon = 10^{-3} \cdot \max\left(\mathbf{S}^{(n)}\right)$ is shown to be proper by numerical experimentation, where $\max\left(\mathbf{S}^{(n)}\right)$ denotes the maximum element of $\mathbf{S}^{(n)}$.

As a further step, to deal with the ill-posedness of the sensing matrix, denoting the SVD of $\bar{\bar{\mathbf{Z}}}$ as $\bar{\bar{\mathbf{Z}}} = \mathbf{U}_Z \mathbf{L}_Z \mathbf{V}_Z^*$, then mapping $\bar{\bar{\mathbf{Z}}}$ onto the matrix $\mathbf{P} = \left(\mathbf{L}_Z^2 + \zeta \mathbf{I}\right)^{-1/2} \mathbf{U}_Z^*$ [13] yields a modified imaging model

$$\mathbf{P}\bar{\mathbf{Y}} = \mathbf{P}\bar{\bar{\mathbf{Z}}}\bar{\mathbf{S}} + \mathbf{P}\bar{\mathbf{N}}, \tag{25}$$

where $\zeta = 10^{-3} \cdot \max\left(\mathbf{L}_Z^2\right)$ is for the ill-conditioned $\mathbf{L}_Z$. Thus $\mathbf{S}$ can be retrieved by solving the l_1-norm optimization problem with $\mathbf{P}\bar{\mathbf{Y}}$ and $\mathbf{P}\bar{\bar{\mathbf{Z}}}$ instead of $\bar{\mathbf{Y}}$ and $\bar{\bar{\mathbf{Z}}}$.

V. Numerical results

Tests are made with a laminate in air composed of an epoxy matrix ($\epsilon = 3.6$, loss tangent $\tan\delta = 0.02$) and graphite fibers ($\epsilon_f = 12$, conductivity $\sigma = 300$ S/m) (just mention that testing of graphite-fibered composites is of much interest [14].)

First, the electromagnetic model is validated with the software COMSOL [15], letting boundaries configured as periodic so as the supercell concept can be simulated. Comparisons are led with $L = 13$, as illustrative example.

Letting $\lambda^{inc} = 10d$ and varying the incident angle from 0 to $\pi/2$, the energy reflection and transmission coefficients as defined in [16], are shown in Fig. 3, and good agreement is observed. With $\theta^{inc} = 0$ and varying the frequency, d/λ^{inc} ranging from 0.01 to 1, results as line graphs in Fig. 4 also show a good fit. Emphasize that, though COMSOL can provide field solutions, the mesh size should be small enough for accuracy, since it runs with a finite-element method, bringing heavy time cost. With $\lambda^{inc} = 10d$ and $\theta^{inc} = \pi/4$, as an example, COMSOL costs 27 times the proposed approach.

A simulation is now designed to test the convergence of the field in the central area of the supercell vs. L. Set 100 equally spaced receivers along the line $z = 2d, -5d \le x \le 5d$. Assume L changes according to formula $(2k+1)$, $k = 1, 2, \ldots$, the convergence can be judged from relative convergence

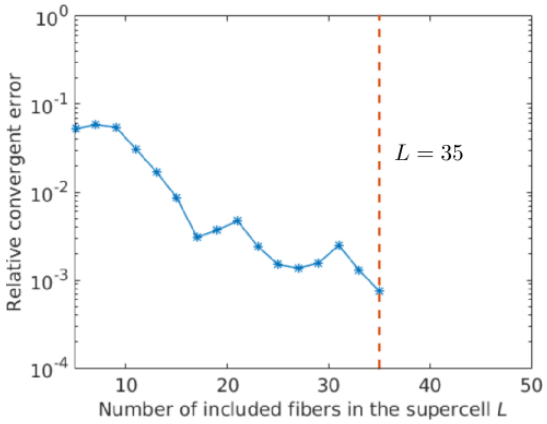

Fig. 5. Convergence of field in central area vs. number of fibers in supercell.

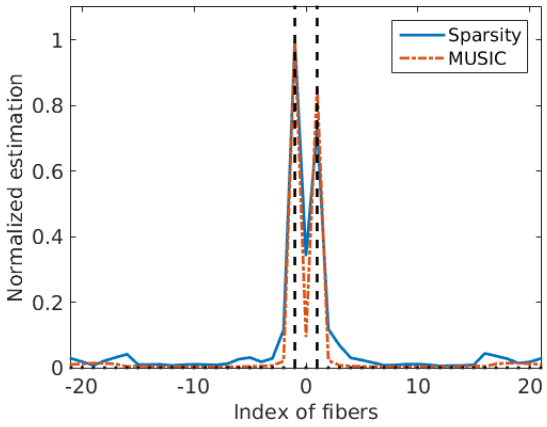

Fig. 6. Imaging of absent fibers with indices -1 and 1.

errors as $\tau_k = \max_j \left|\vec{\psi}_{k+1}^j - \vec{\psi}_k^j\right| / \left|\vec{\psi}_{k+1}^j\right|$, where $\vec{\psi}_k^j$ denote the data collected by the j-th receiver when $L = (2k+1)$. The field is said to be convergent if τ_k is below 10^{-3}.

Simulation results vs. $\lambda^{inc} = 10d$ are shown in Fig. 5. Relative errors have fluctuations but keep the descent direction with increased L and the convergence number is seen as 35.

Taking $L = 43$, somewhat larger than 35 for safety, 4 plane

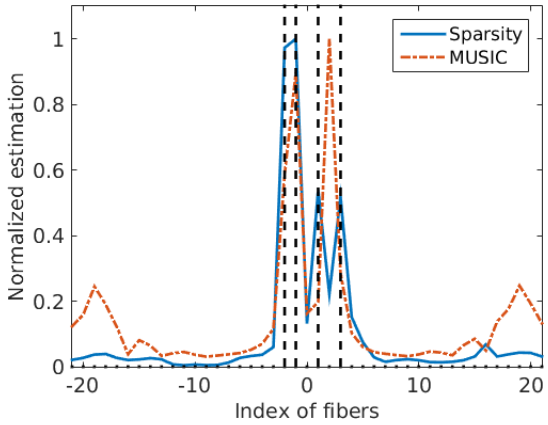

Fig. 7. Imaging of absent fibers with indices $[-2,-1,1,3]$.

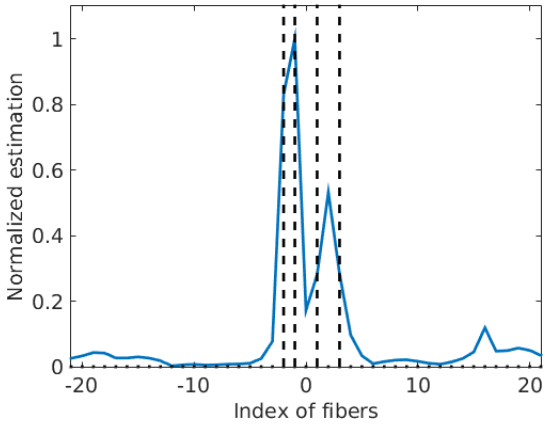

Fig. 8. Estimation of absent fibers of indices -1 and 1 without preprocessing.

waves with angles $[-\pi/3,-\pi/4,-\pi/6,0]$ and 20 equally-spaced receivers along the line $z=2d, -5d \leq x \leq 5d$ are chosen to image the absent fibers. Gaussian noise is added with 30 dB signal to noise ratio. Sparsity-based reconstruction is run with parameters $\tau = 0.01$, and the quantity displayed is the vector $\hat{\mathbf{s}} = [||\mathbf{S}^l||_2]$, $\mathbf{S}^l$ the l-th row of $\mathbf{S}$.

Assuming fibers with indices from -23 to 23, estimation of absent fibers with indices -1 and 1 is illustrated in Fig. 6 where vertical dashed lines denote the right solution. Both MUSIC and sparsity-based algorithm (marked as Sparsity) can well retrieve the location of missing fibers.

Increase of their number to 4 with indices $[-2,-1,1,3]$ leads to the result shown in Fig. 7. Missing fibers 1 and 3 merge as one peak with MUSIC, while they can be well distinguished by the iterative sparsity-based approach.

As for the effect of preprocessing in (25), an imaging result of sparsity-based algorithm without it is given in Fig. 8 which shows the -1st and 1-st fiber are not correctly detected.

VI. Conclusion

Investigations about fibered laminates with missing fibers are performed. An auxiliary periodic structure with supercell unit is introduced so that the field analysis can be operated with methods tailored for periodic structures. To locate the missing fibers, imaging models are derived from a Lippman-Schwinger integral formulation, and simplified by using a zero-mode approximation.

Both standard MUSIC and iterative methods within implicit (MUSIC) or explicit (iterative solution) sparsity contexts are applied to locate the missing fibers (in effect, a distribution of index in a succession). However, for the sparsity-based approach, the structure of $\mathbf{S}$, *i.e.* exhibiting a few non-zero rows, is lost after the vectorization. In [17], the sparsity of the covariance matrix is exploited in direction of arrival estimation, and work along that line is to be envisaged..

Investigations on the multilayer structure with fibers possibly missing in several layers are also foreseen. In addition, how do homogenization methods —which in properly chosen operation frequency bands and for possibly specific materials make the missing fibers look like small isolated scatterers within a homogenized slab medium— compare with previous results in terrms of imaging and resolution is to be considered.

References

[1] C. Y. Li, D. Lesselier and Y. Zhong, "Recursive matrix schemes for composite laminates under plane-wave and Gaussian beam illumination," J. Opt. Soc. Amer. B., vol. 32, pp. 1539-1549, 2015.
[2] J.-P. Groby and D. Lesselier, "Localization and characterization of simple defects in finite-sized photonic crystals," J. Optical Soc. Amer. A, vol. 25, pp. 146-152, 2008.
[3] A. Brancaccio, G. Leone and R. Solimene, "Fault detection in metallic grid scattering, J. Opt. Soc. Amer. A, vol. 28, pp. 2588-2599, 2011.
[4] Z. C. Liu, C. Y. Li, D. Lesselier and Y. Zhong, "Electromagnetic modeling of a periodic array of fibers embedded in a panel with single fiber missing," in Electromagnetic Non-Destructive Evaluation (XIX), N.Yusa *et al.* eds, IOS Press, Amsterdam, in press, 2016.
[5] J.-P. Groby *et al.*, "Acoustic response of a rigid-frame porous medium plate with a periodic set of inclusions, J. Acoust. Soc. Amer., vol. 126, pp. 685-693, 2009.
[6] R. G. Baraniuk, "Compressive sensing," IEEE Signal Proc. Mag., vol. 24, pp. 118-121, 2007.
[7] C. Y. Li, D. Lesselier and Y. Zhong, "Electromagnetic small-scale modeling of composite panels involving periodic arrays of circular fibers, Appl. Phys. A, vol. 117, pp. 567-572, 2014.
[8] L. C. Botten *et al.*, "Formulation for electromagnetic scattering and propagation through grating stacks of metallic and dielectric cylinders for photonic crystal calculations. Part I. Method, J. Opt. Soc. Am. A, vol. 126, pp. 2165-2176, 2000.
[9] H. Ammari *et al.*, Mathematical and Statistical Methods for Multistatic Imaging, Lect. Notes Math. vol. 2098, Springer, Heidelberg, 2013.
[10] P. C. Hansen, T. K. Jensen, and G. Rodriguez, "An adaptive pruning algorithm for the discrete l-curve criterion," J. Comput. Appl. Math., vol. 198, pp. 483-492, 2007.
[11] D. P. Bovet and P. Crescenzi, Introduction to the Theory of Complexity. Prentice Hall, 1994.
[12] E. J. Candès, J. Romberg, and T. Tao, "Robust uncertainty principles: Exact signal reconstruction from highly incomplete frequency information," IEEE Trans., Inform. Theory, vol. 52, pp. 489-509, 2006.
[13] O. K. Lee, H. Kang, J. C. Ye, and M. Lim, "A non-iterative method for the electrical impedance tomography based on joint sparse recovery," Inverse Probl., vol. 31, 075002 (23pp), 2015.
[14] H. Heuer *et al.*, "Review on quality assurance along the CFRP value chain-Nondestructive testing of fabrics, preforms and CFRP by HF radio wave techniques," Composites Part B, vol. 77, pp. 494-501, 2015.
[15] https://www.comsol.com/model/plasmonic-wire-grating-10032
[16] A. K. Kong, Electromagnetic Wave Theory. EMW Publishing, 2000.
[17] P. Stoica, B. Prabhu, and J. Li. "SPICE: A sparse covariance-based estimation method for array processing," IEEE Trans., Signal Proc., vol. 59, pp. 629-638, 2011.